communications biology

Article

https://doi.org/10.1038/s42003-024-07133-1

NMR investigation of FOXO4-DNA interaction for discriminating target and non-target DNA sequences

Donghoon Kang[1,3], Min June Yang[1,3], Hae-Kap Cheong[2] & Chin-Ju Park[1]

Forkhead box O4 (FOXO4), a human transcription factor, recognizes target DNA through its forkhead domain (FHD) while maintaining comparable binding affinity to non-target DNA. The conserved region 3 (CR3), a transactivation domain, modulates DNA binding kinetics to FHD and contributes to target DNA selection, but the underlying mechanism of this selection remains elusive. Using paramagnetic relaxation enhancement analysis, we observed a minor state of CR3 close to FHD in the presence of non-target DNA, a state absent when FHD interacts with target DNA. This minor state suggests that CR3 effectively masks the non-target DNA-binding interface on FHD. The interaction weakens significantly under high salt concentration, implying that CR3 or high salt concentrations can modulate electrostatic interactions with non-target DNA. Our ^{15}N relaxation measurements revealed FHD's flexibility with non-target DNA and increased rigidity with target DNA binding. Our findings offer insights into the role of FOXO4 as a transcription initiator.

In eukaryotic cells, each transcription factor (TF) recognizes its own target DNA sequence to regulate gene expression. TFs move within the nucleus by Brownian motion and approach DNA to bind to a target gene sequence[1]. Then, TFs quickly scan countless non-target DNAs through 1D sliding and hopping/jumping strategies until they reach their target DNA[1]. For this purpose, most TFs require a certain level of affinity with non-target DNA.

The human genome comprises approximately 1600 TFs, of which about 50 are members of the forkhead box (FOX) family[2]. FOX class O proteins (FOXO), a family of human TFs that shares the forkhead DNA-binding domain (FHD)[3–5], participate in various cellular processes such as cell cycle regulation, cell survival, metabolism, inflammation, differentiation, stress resistance, apoptosis, and tumorigenesis[6–14]. These processes impact carcinogenesis, diabetes, complications related to diabetes, cardiovascular disease, host response, and healing of wounds[14]. FOXOs are also known as important cellular senescence regulators[15]. Among the four human FOXO TFs (FOXO1, FOXO3a, FOXO4, and FOXO6)[16,17], FOXO4 is highly expressed in muscle and heart tissue[18]. FOXOs regulate their transcriptional activity through post-translational modifications such as phosphorylation, ubiquitination, methylation, and acetylation[10,19–22]. Acetylation of K186, K189, and K408 induces the export of FOXO4 from the nucleus, reducing the transcriptional activity of FOXO4[14,23].

FOXOs contain several domains, including the FHD, a nuclear localization sequence (NLS), a nuclear export sequence (NES), and a transactivation domain at the C-terminus (conserved region 3; CR3) (Fig. 1a). FOXO4 FHD is known to recognize specific DNA sequences known as the DAF-16 family member-binding element (DBE) and insulin-responsive element, like other FOXs[24,25]. Flanking sequences facilitate DNA binding to mouse FOXO1[25,26]. The structure of FOXO4 FHD in complex with its target DNA was determined using X-ray crystallography[27] (Fig. 1b). It showed that helix 3 (H3) of FHD interacted with the bases of the target DNA, and the N-terminus and wing 1 (W1) regions interacted with the phosphate backbone of the target DNA. Figure 1c shows the target DNA sequence that was used and the random non-target sequence[28]. It is known that TFs have a relatively higher binding affinity for target DNA compared to non-target DNA, as exemplified by p53, pre-B-cell leukemia TF 1, and homeobox protein A[13,29–31]. Additionally, TFs often undergo homo- or hetero-multimerization to increase target binding ability[32,33]. For example, FOXO1 binds to specific DNA sites as a homodimer[34], and FOXP3 forms a heterodimer with a nuclear factor of activated T cells for DNA binding[35–38].

Unlike other TFs, FOXO4 FHD binds its target DNA as a monomer, and binds to both target and non-target DNAs with a similar level of affinity, using a similar binding interface in vitro[28]. Under high salt buffer conditions, the dissociation constant (K_d) for both types of DNAs was similarly weakened[28]. These observations imply that FOXO4 FHD itself does not achieve high selectivity for its cognate DNA sequence. It was previously suggested that FOXO4 FHD obtains DNA selectivity possibly via intramolecular interaction with FOXO4 CR3, which is negatively charged and intrinsically disordered, such that FOXO4 CR3 effectively competes with

[1]Department of Chemistry, Gwangju Institute of Science and Technology, Gwangju, 61005, Republic of Korea. [2]Ochang Center, Korea Basic Science Institute, Chungcheongbuk-do, 28119, Republic of Korea. [3]These authors contributed equally: Donghoon Kang, Min June Yang. e-mail: cjpark@gist.ac.kr

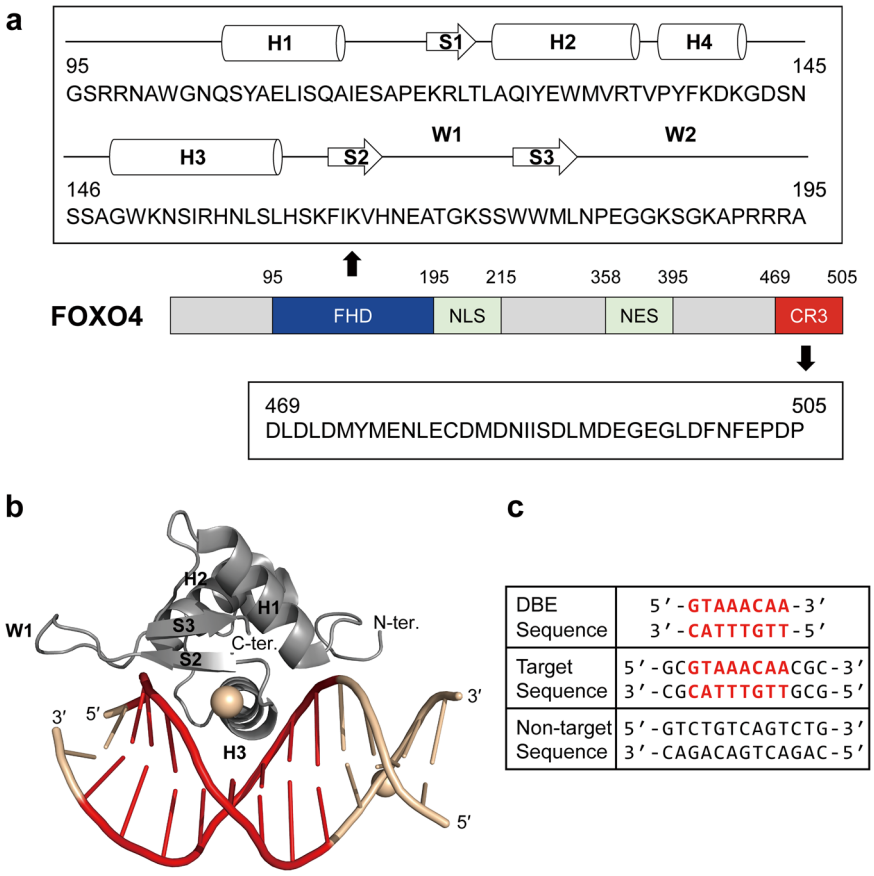

Fig. 1 | Structure of FOXO4 and oligomeric DNA sequences. a Domain structure of FOXO4. Primary sequences of FOXO4 FHD and CR3 are illustrated with arrow-marked extensions. **b** Complex structure of FOXO4 FHD and DAF-16 family member-binding element (DBE; PDB ID: 3L2C)[27]. DBE sequences are shown in red. **c** DBE, target, and non-target DNA sequences. DBE sequences are shown in red.

non-target DNA for FHD interaction and induces fast exchange between the free and DNA-bound states of FHD[28]. A similar intramolecular interaction occurs between the transactivation domain and the DNA-binding domain of p53, and it reduces the binding affinity of p53 for non-target DNA sequences[31].

Even though it is known that CR3 plays a crucial role in the target DNA recognition of FOXO4 FHD, it is still unclear how FOXO4 distinguishes its target DNA from large amounts of non-target DNA in the nucleus. To address this question, we investigated the structural and dynamic aspects of the FHD–DNA complex in various conditions using NMR techniques. We found through NMR paramagnetic relaxation enhancement (PRE) experiments that the distance between CR3 and FHD is different depending on the presence of either target or non-target DNA. We also performed comparative chemical shift perturbation (CSP) analyses of the wild-type FHD and a C-terminus deletion mutant with two DNAs in different salt conditions. With this systematic approach, we illustrate features of the DNA interface of FHD that distinguish target and non-target DNA at the residue level. Finally, we observed different backbone dynamics of FHD in the unbound, target DNA-bound, and non-target DNA-bound states. Based on our findings, we propose that despite having minimal secondary structure, the positively charged C-terminus region of FHD plays a crucial role in its interaction with DNA and CR3. While most studies of TFs mainly focus on explaining their interactions with target DNA, the current study provides important insights into transcriptional regulation by the FOX family of TFs and reveals the functions of various structural domains of FOXO4 through the study of its interactions with target DNA as well as non-target DNA.

Results

CR3 affects FHD in the presence of non-target DNA

We previously revealed that the interaction between CR3 and FHD affects the dynamic properties of the FHD depending on the DNA sequence[28]. In addition, an NMR structural study of the FHD-CR3 complex demonstrated that CR3 occupied the DNA-binding surface of FHD[28,39]. While the presence of CR3 causes lower binding affinities and faster exchange of the FHD with non-target DNA, it rarely changes the exchange rate for target DNA. These dynamic differences suggest that CR3 modulates FOXO4-target DNA recognition[28]. To investigate the role of CR3 in the interaction between FHD and DNA, we conducted PRE experiments to measure the relative distances between FHD, CR3, and DNA.

Initially, we performed PRE experiments with S-(1-oxyl-2,2,5,5-tetramethyl-2,5-dihydro-1H-pyrrol-3-yl)methyl methanesulfonothioate (MTSL) labeling on C481 in CR3 to examine the interaction between FHD and CR3. As shown in Fig. 2a, several residues within the helices of FHD exhibited a reduction in intensity ratio (intensity of oxidized state ($I_{paramagnetic}$)/intensity of reduced state ($I_{diamagnetic}$) < 0.50), consistent with the CSP analysis and structural model from previous studies (Supplementary Fig. 1)[28,39]. This showed that CR3 is predicted to share the binding site with DNA, bringing CR3 into proximity with the helices of FHD, as indicated by the PRE results.

Next, the interaction between FHD and CR3 in the presence of target DNA was investigated. Unlike the results obtained in the absence of DNA, no appreciable decrease in intensity ratio was observed (Fig. 2b). This implies that the presence of target DNA significantly impeded the interaction between FHD and CR3, so CR3 does not come within 25 Å of FHD[40]. We then observed the interaction between FHD and CR3 in the presence of non-target DNA. A discernible decrease in intensity ratios within the sheet 2 (S2)–W1 region was observed (Fig. 2c), showing that CR3 affects FHD in the presence of non-target DNA. This contrasts with the results in the presence of target DNA, suggesting that the interaction between FHD and CR3 is affected differently by different DNA sequences. We also quantitatively measured the PRE rate (^1H_N–Γ_2). As previously noted, ^1H_N–Γ_2 values exceeding 10 s^{-1} are significant[41]. Notably, the region exhibiting ^1H_N–Γ_2 values greater than 10 s^{-1} was observed only in the presence of non-target DNA but not with target DNA (Supplementary Fig. 2). These findings

suggest that when FOXO4 FHD is bound to non-target DNA, CR3 affects the helix 1, helix 2, S2, and sheet 3 regions of FHD. Considering the similar K_ds of FHD for both types of DNA but a higher exchange rate for the non-target DNA in the presence of CR3[28], the apparent PREs observed in the FHD-non-target DNA system by MTSL-labeled CR3 might result from a minor state in which FHD is closer to CR3, whereas the major DNA-bound conformation might be similar to the target DNA-bound form of FHD.

Notably, both types of DNA could release CR3 from FHD based on previous $^{1}H–^{15}N$ heteronuclear single quantum coherence (HSQC) monitoring[28]. By measuring PRE, we observed that CR3 is not completely dissociated from the FHD-non-target DNA complex. In particular, some portions of CR3 could be transiently located close to the S2–W1 region rather than the H3 regions of FHD, which are the main CR3 binding sites. This is likely due to the occupation of FHD's H3 regions by DNA, making it easier for CR3 to interact with S2–W1 of FHD, which is relatively weakly occupied by non-target DNA.

FHD-non-target DNA interaction experiences fast exchange under the high salt concentration

To answer the question of how CR3 competes better with the non-target DNA than the target DNA for FHD binding, we hypothesized that CR3, with its abundance of negatively charged residues, could effectively impede the less-specific electrostatic interactions between non-target DNA and FHD. In order to examine this hypothesis, we tested FHD–DNA interaction without CR3 under high salt concentration. We performed $^{1}H–^{15}N$ HSQC titration experiments of FHD with the target and non-target DNA at 50 and 150 mM NaCl. Figure 3a, b shows the CSP graphs of ^{15}N labeled FHD with target and with non-target DNA in 50 mM NaCl buffer, respectively. While overall CSP changes are higher in target DNA, the significantly perturbed residues (>2 standard deviations), such as A107 in the N-terminus, R155 in H3, and N169 and W178 in the C-terminus are the same between the target and non-target DNA titrations. This confirms that the N-terminus, H3, and C-terminus regions play a crucial role in DNA interaction. Under 150 mM NaCl conditions, the CSPs caused by the target DNA titration were not significantly changed, and the mean of the CSP values ($\Delta\delta_{avg}$) was also similar (Fig. 3a, c; 0.133 and 0.140 ppm). Y106, A107, V167, and N169 still maintained high $\Delta\delta_{avg}$s with target DNA even at high salt concentrations. There was a slight decrease of N152 and R155 CSP in the H3 region, which is known to directly interact with DNA. In the case of non-target DNA at high salt, the mean of $\Delta\delta_{avg}$ was reduced from 0.092 to 0.073 ppm (Fig. 3b, d). The decreases in CSPs in H3 (N152, R155, and L158) and S2–W1 (F164, K166, H168, and N169) were significant. In particular, the positively charged sidechains of K166 and H168 in S2 could be involved in electrostatic interaction with the DNA backbone.

We also found that the exchange rate of non-target DNA–FHD binding was affected by high NaCl concentration. A107 in H1 and V167 in S2 are well separated, with fast and slow exchange clearly distinguishable, and were monitored with increasing DNA concentrations. With target DNA, the peaks of the unbound state disappeared and then reappeared at the bound position in both 50 and 150 mM NaCl (Fig. 4a–d). With non-target DNA, the peaks showed intensity decreasing and peak broadening under the half ratio of DNA adding to the FHD condition, which is slow-to-intermediate exchange behaviors in 50 mM NaCl (Fig. 4e, f). However, they showed gradual shifts with non-target DNA in 150 mM NaCl (Fig. 4g, h). This implies that FHD binding to non-target DNA undergoes fast exchange at high salt concentrations. The previous study showed that the presence of CR3 changes the exchange rate of non-target DNA–FHD binding[28]. Taken together, we suggest that the presence of CR3 and/or high salt contributes to the selective DNA binding of FOXO4 by reducing the less-specific electrostatic interaction between FHD and non-target DNA.

Lastly, we investigated whether the non-target DNA can compete with the target DNA for FHD binding. Two samples were prepared for this experiment. The first sample was prepared by mixing the target DNA with FHD, followed by adding non-target DNA (Supplementary Fig. 3a). In the second sample, FHD was mixed with non-target DNA first, and then target DNA was added (Supplementary Fig. 3b). The samples were incubated for more than 18 h at 4 °C, in 50 mM NaCl buffer. Supplementary Fig. 3 shows that most of the peaks in the presence of both types of DNA were in a similar position to that of the target DNA-bound form, regardless of the order of addition. Notably, the target DNA inhibited non-target DNA binding to FHD, even when the non-target DNA was already bound to FHD. This indicates that non-target DNA does not effectively compete with target DNA for FHD binding, suggesting the FHD–target DNA complex is stable.

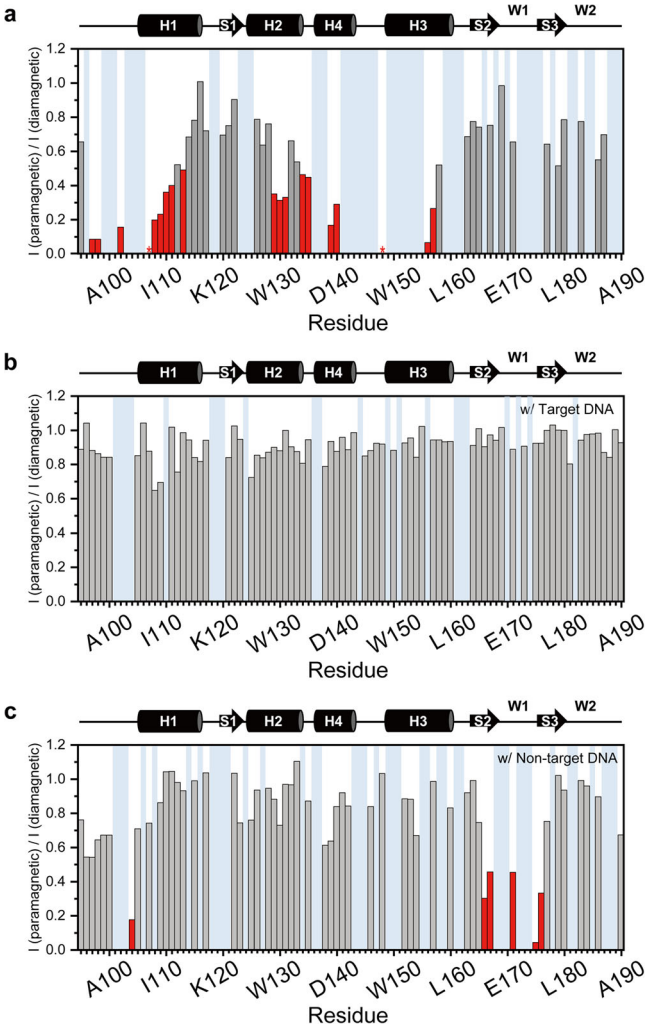

Fig. 2 | Results of PRE experiments between MTSL-labeled CR3 and FHD. Plots of intensity ratio ($I_{paramagnetic}/I_{diamagnetic}$) of FHD signals against its residue number are shown for FHD in complex with CR3 modified with MTSL at C481 **a** without DNA, **b** with target DNA, and **c** with non-target DNA. Bars corresponding to residues with significant intensity reductions ($I_{paramagnetic}/I_{diamagnetic} < 0.50$) are colored red. Asterisks (*) indicate residues that broadened out under the influence of MTSL. Light blue bars indicate unassigned residues.

FHD is more flexible when interacting with non-target DNA

Our PRE and CSP analyses showed that the S2–W1 region of FHD is sensitive to the salt concentration for the non-target DNA binding and is involved in CR3 interaction in the presence of non-target DNA. The C-terminus region (W2) of FHD is also known to be crucial for DNA binding[42] and contains several positively charged residues. Because these regions lack secondary structure, studying their involvement in DNA interaction is challenging through static complex structures. Also, the aggregation was monitored in the non-target DNA–FHD mixture, which hindered further study of the complex structure. In order to compare the dynamic behavior of the unbound state with the target DNA-bound and

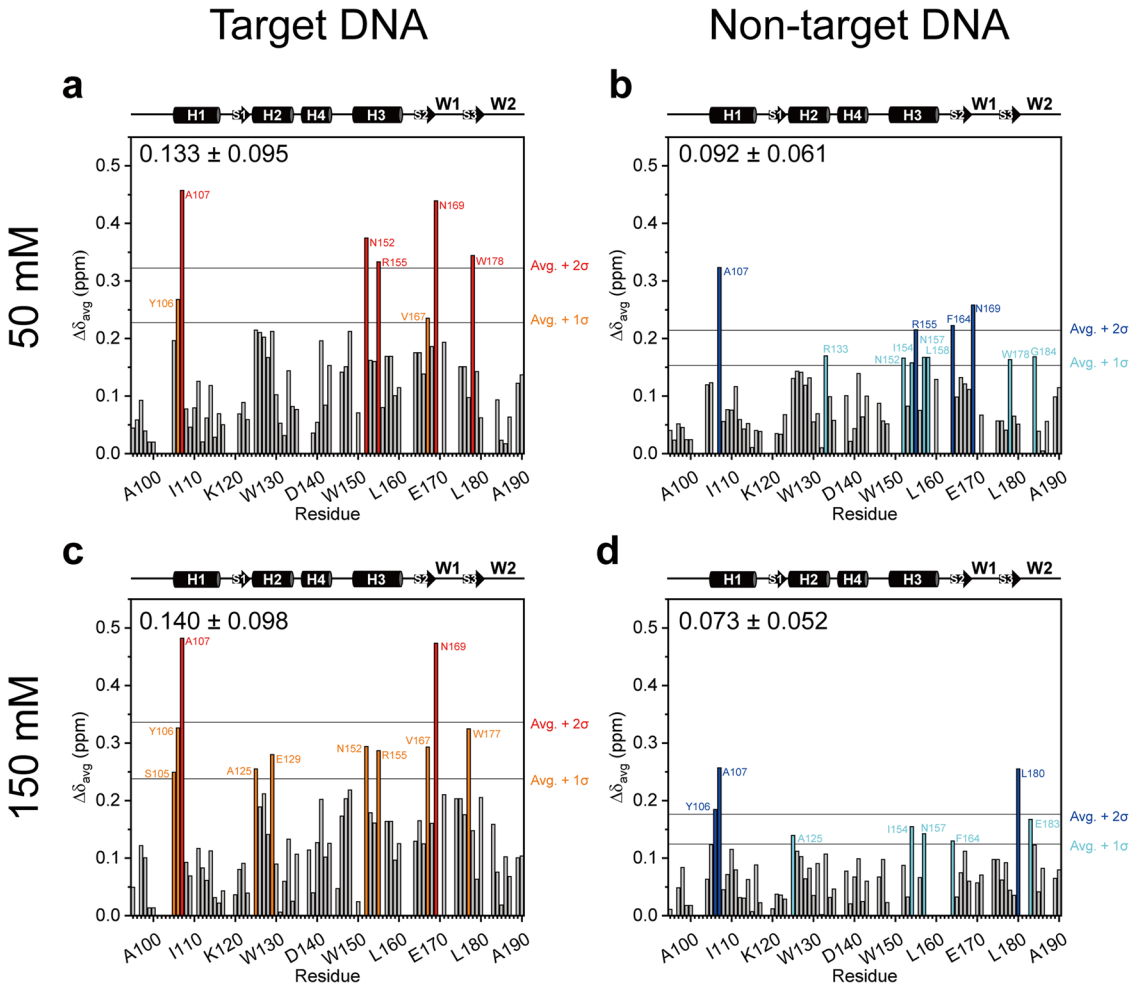

Fig. 3 | Average chemical shift perturbation ($\Delta\delta_{avg}$) of ^{15}N-labeled FOXO4 FHD. $\Delta\delta_{avg}$ of FOXO4 FHD titrated at 50 mM NaCl (**a**, **b**) or 150 mM NaCl (**c**, **d**) with target (**a**, **c**) or non-target DNA (**b**, **d**). CSPs were calculated from the difference between FOXO4 FHD and DNA ratios of 1:0 and 1:2. Residues with CSPs >2 standard deviations larger than average are shown in red or blue, and residues >1 standard deviation larger than average are shown in orange or cyan. Each average ± standard deviation is displayed in the upper left corner.

non-target DNA-bound states, we measured the ^{1}H-^{15}N backbone dynamics by collecting the ^{15}N spin relaxation parameters (heteronuclear nuclear overhauser effect; hetNOE, spin–lattice relaxation; R_1, and spin–spin relaxation; R_2) of each state.

In the unbound state, the N-terminus, W1, and W2 of FHD exhibited low hetNOE values (<0.6)[43,44], which indicates this region is flexible (Fig. 5a). Conversely, in the target DNA-bound state (Fig. 5a, left), these regions showed significantly higher hetNOE values compared to their unbound state. This observation implies a notable increase in rigidity in these specific regions upon DNA binding, strongly indicating their critical role in DNA-binding interactions. In the non-target DNA-bound state, the hetNOE values for the N-terminus and W2 increased compared to the unbound state (Fig. 5a, right). However, in the S2–W1 region, the values were similar to the unbound state or decreased. In general, as with the target DNA results, the value should increase due to DNA binding, but similar or lower values imply that these regions are not likely to be involved in binding. This suggests that the N-terminus and W2 contribute to non-target DNA binding, while S2–W1 does not play a significant role in this binding process (Fig. 5b, left).

We also noted substantial differences in R_1 and R_2 values of the S2–W1 region of FHD depending on the DNA sequence. Specifically, in the FHD–target DNA complex, the S2–W1 region exhibited an increase in R_2 and hetNOE values, along with a decrease in R_1 values, compared to the unbound state (Fig. 5, Supplementary Fig. 4, and Table 1). In contrast, for the FHD-non-target DNA complex, it was observed that the R_1, R_2, and hetNOE values remained similar to those of the unbound state. This indicates that the S2–W1 retains flexibility and dynamic motion despite being bound to non-target DNA. Consequently, the S2–W1 is a region exclusively involved in binding to target DNA, consistent with our PRE results. Furthermore, in the case of the N-terminus and W2, irrespective of the DNA sequence, it was observed that the hetNOE value of FHD increased when DNA was present. This suggests that the N-terminus and W2 do not exhibit sequence specificity towards DNA but are crucial for FHD's overall DNA-binding ability.

Additionally, our results show that FHD–DNA complexes exhibit different levels of rotational correlation time (τ_c) depending on the DNA sequence, even when DNA molecules of the same molecular weight are bound. The FHD–target DNA complex showed a longer τ_c than the FHD–non-target DNA complex (Supplementary Table 1). This is attributed to FHD adopting a rigid complex with target DNA, resulting in a larger molecular assembly. Conversely, the FHD–non-target DNA complex forms a relatively less rigid structure, allowing for more separation than the FHD–target DNA complex. Despite having the same molecular weight as the FHD–target DNA complex, it exhibits shorter τ_cs. These conformational properties are consistent with the hetNOE average value.

The C-terminus of FHD is essential for non-target DNA binding

As we mentioned previously, the W2 region in the C-terminus contains positively charged residues, which mediate electrostatic interaction with the DNA backbone. Because electrostatic interactions are more easily weakened by high salt, or the presence of CR3, we hypothesized that C-terminus

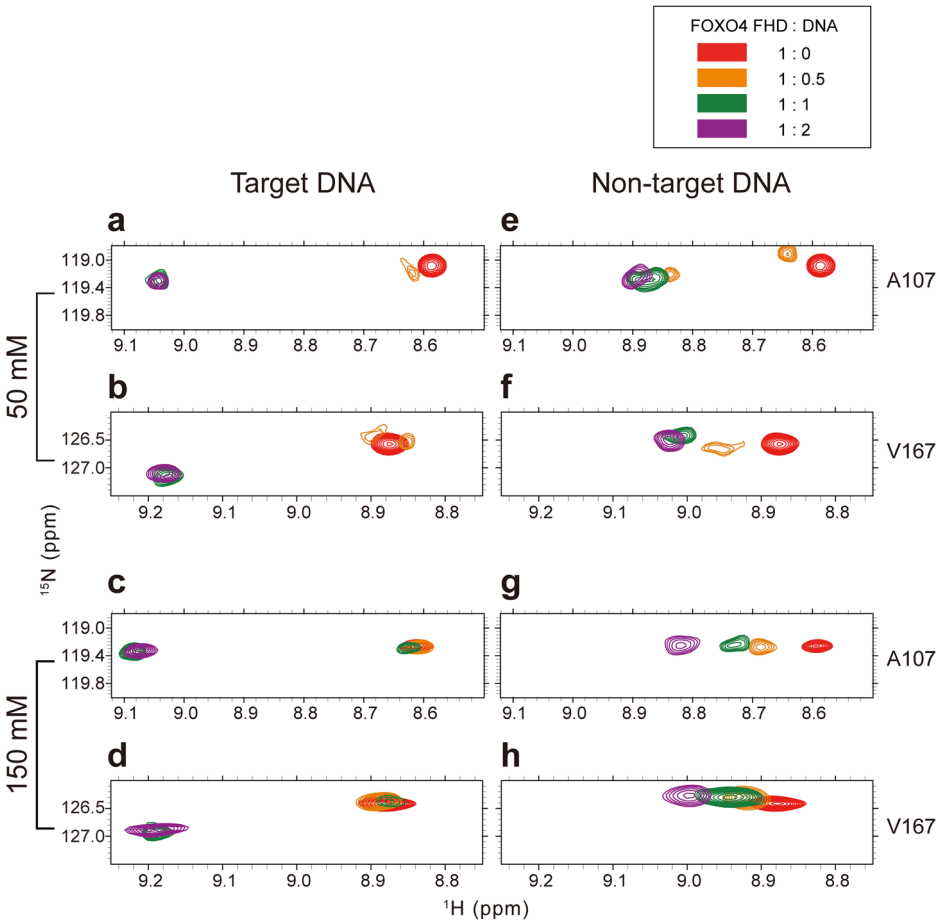

Fig. 4 | ^{15}N HSQC spectra of FOXO4 FHD A107 and V167. ^{15}N HSQC spectra of FOXO4 FHD titrated with target (**a**–**d**) and non-target DNA (**e**–**h**) at 0 (red), 0.5 (orange), 1 (green), and 2 (purple) molar ratio under 50 mM NaCl (**a**, **b**, **e**, **f**) and 150 mM NaCl (**c**, **d**, **g**, **h**) buffer conditions. Peaks of residues A107 (**a**, **c**, **e**, **g**) and V167 (**b**, **d**, **f**, **h**) are shown.

truncation would affect DNA binding distinctively depending on the DNA sequence. To determine the role of the C-terminus region of FHD in DNA binding, we prepared a C-terminus truncation mutant (FHD_ΔW2; 95–183 amino acids (a.a.)). First, we compared the ^{1}H–^{15}N HSQC spectra of FHD WT and FHD_ΔW2 to verify that truncation of the C-terminus region did not cause any structural loss in FHD. Most peaks overlapped, confirming that truncation did not affect the overall structure of FHD (Supplementary Fig. 5). We performed ^{1}H–^{15}N HSQC titration experiments of FHD_ΔW2 in the presence of target and non-target DNA under 50 mM or 150 mM NaCl concentrations. Figure 6a shows the CSP patterns of FHD_ΔW2 were similar to those of wild-type FHD (Fig. 3a). $\Delta\delta_{avg}$s of FHD_ΔW2 with target DNA were 0.127 and 0.141 ppm under 50 and 150 mM NaCl conditions, respectively, similar to those of wild-type FHD (Figs. 3a, c and 6a, c).

In the case of non-target DNA titration, the magnitude of CSPs of FHD_ΔW2 was significantly reduced compared to the wild-type (Fig. 6b). $\Delta\delta_{avg}$s of FHD_ΔW2 with non-target DNA were 0.049 ppm under 50 mM NaCl, about half of FHD wild-type (0.092 ppm) (Fig. 3b). Except for the W2 region, other DNA interfaces were mostly maintained. These data show that the C-terminus region is unnecessary for target DNA binding. Among the non-target DNA interface, the S2–W1 region was not perturbed in FHD_ΔW2 (Fig. 6b, d) compared with the CSP results of FHD_ΔW2 with target DNA (Fig. 6a, c). It is noteworthy that the S2–W1 region was perturbed by non-target DNA in wild-type FHD 50 mM NaCl (Fig. 3b). This implies that the C-terminus of FHD is essential for the non-target DNA interaction, and it contributes to maintaining the S2–W1 interface with the DNA.

Our monitoring of A107 in H1 and V167 in S2 of FHD_ΔW2 with increasing DNA concentrations is shown in Supplementary Fig. 6. With target DNA, both peaks showed slow to intermediate exchange regardless of NaCl concentrations (Supplementary Fig. 6a–d). In the case of non-target DNA titration, both peaks shifted gradually, even under 50 mM NaCl concentration (Supplementary Fig. 6e–h). Because the equivalent peaks showed slow to intermediate exchange under 50 mM NaCl (Fig. 4e, f), it implies that the C-terminus truncation affects the exchange rate for non-target DNA at the low salt condition. Taken together, our data demonstrate that the W2 region, which mediates nonspecific electrostatic interaction with DNA, contributes more to non-target DNA binding, whereas target DNA recognition is less affected by blocking the electrostatic interaction with the high salt or C-terminus deletion.

Discussion

FOXO4 controls cellular balance via specific promoter interactions, and its dysregulation strongly correlates with multiple cancers, aging-related diseases, and senescence[24,45]. FOXO4 interacts with both target and non-target DNA through similar surfaces and binds each with comparable affinity (Fig. 3a, b, and Supplementary Fig. 7). However, the mechanism by which FOXO4 distinguishes between target and non-target DNA has not yet been elucidated. Our NMR investigation of the FOXO4-DNA interaction showed the possibility of a minor state in the FOXO4-non-target DNA system. In the presence of non-target DNA, recognition helix H3 was not affected by CR3, indicating that this region maintained its interaction with the DNA. Instead, other parts of FHD showed decreased intensities and apparent $^{1}H_N$–Γ_2 values (Fig. 2c and Supplementary Fig. 2).

In several TFs, intrinsically disordered regions such as transactivation domains are mainly composed of negative charges and are known to accelerate target DNA search by masking the DNA-binding domain[46]. This phenomenon, in which transcription factors such as p53, ETV4, and ERG regulate their own DNA-binding abilities, is an autoinhibitory mechanism[31,47,48]. Autoinhibition occurs when another domain within a protein interacts with the DNA-binding domain (DBD) to prevent DNA binding. The NTAD of p53, the N- and C-terminal inhibitory domains of ETV4, and the flanking regions of the ETS domain in ERG factors could mediate the autoinhibition. FOXO4 is also considered to have an

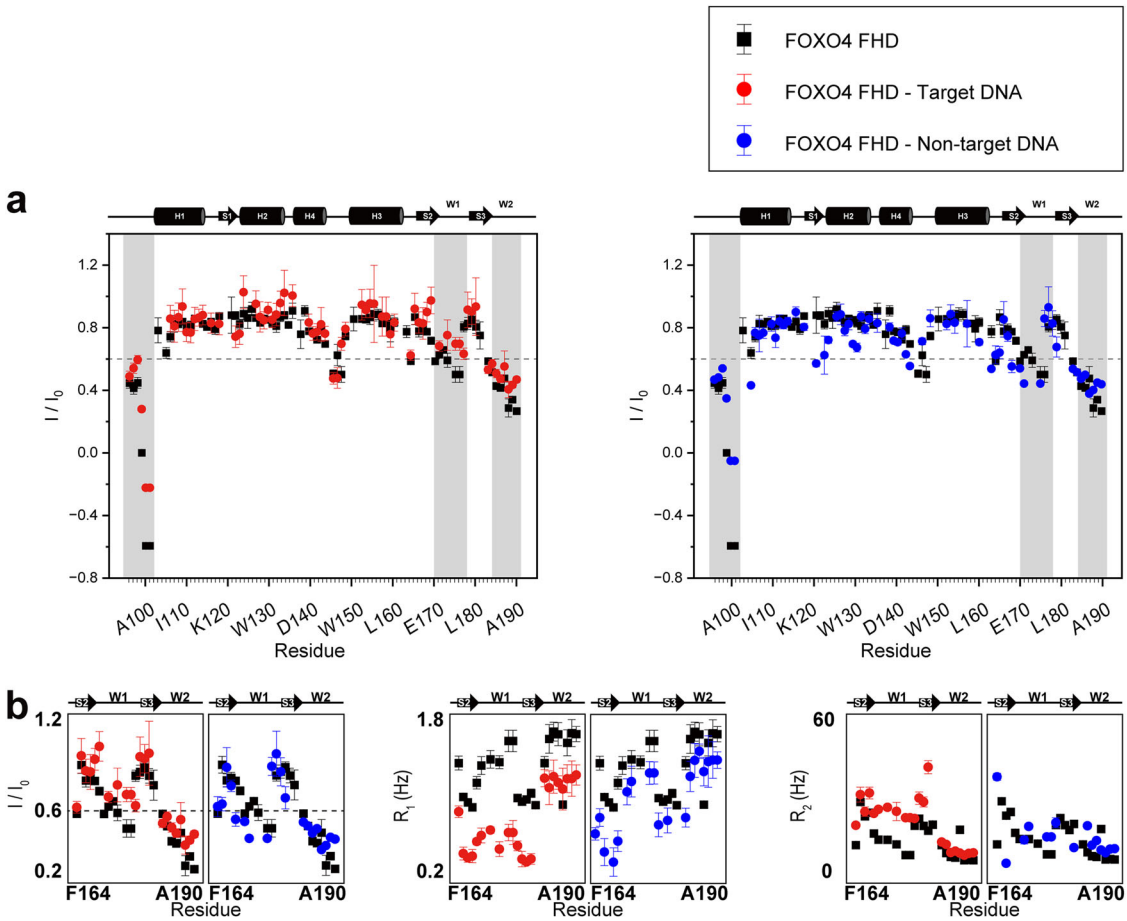

Fig. 5 | FOXO4 FHD backbone dynamics. a Per residue hetNOE of FOXO4 FHD. hetNOE value 0.6 is indicated with a black dotted line. The unstructured region is indicated in the shaded area (gray). **b** Backbone dynamics in C-terminus of FOXO4 FHD. Per residue (left) hetNOE, (middle) R_1, and (right) R_2. Data series correspond to the unbound state of FHD (black), the presence of target DNA (red), and the presence of non-target DNA (blue).

autoinhibitory mechanism through the CR3–FHD interaction. CR3 is presumed to accelerate the exchange rate by interfering with FHD interactions with non-target DNA sequences[28]. Notably, the S2–W1 region of FHD exhibits weak interactions with non-target DNA and is exposed to facilitate CR3 binding. This exposed S2–W1 region likely interacts with CR3. This region is assumed to be involved in different interaction modes depending on the DNA sequence. In this regard, CR3–FHD interaction could be considered to inhibit unnecessary assembly of TF machinery and contribute to rapid target DNA search. Conversely, when FOXO4 binds to the target DNA, it is expected that CR3 is completely dissociated from FHD and able to recruit other TFs and coactivators.

By examining DNA interactions of FHD at high salt conditions, we also demonstrate that the non-target DNA–FHD interaction is mainly governed by electrostatic interaction (Fig. 3). For target DNA recognition, specific DNA bases and the negative phosphate atoms of DNA backbones are generally involved in the TF binding. However, TFs primarily bind with the phosphate backbones for non-target DNA contacts[49,50]. The less-specific non-target DNA interaction is also monitored by measurement of relaxation parameters. While the target DNA-bound form of FHD showed dramatic changes in average values of R_1, R_2, and hetNOE, the non-target DNA-bound form of FHD maintains a similar range of values with the free FHD (Table 1). It is particularly noticeable in the S2–W1 region, where the CR3 interface is in the presence of non-target DNA. It suggests that FHD tends to have a less rigid conformation when interacting with non-target DNA, and the S2–W1 region specifically contributes to target DNA recognition of FHD. Also, we identified that the N- and C- terminus of FOXO4 FHD play a crucial role in interacting with both types of DNAs based on their hetNOE values, which were significantly elevated upon DNA binding (Fig. 5). This is consistent with the fact that these regions interact with the phosphate backbone of DNA from the complex structure and simulation of FOXO4 FHD and target DNA[27,51]. These intrinsically disordered regions are believed to contribute to efficient DNA exploration by promoting brachiation dynamics of intersegment transfer[52].

Table 1 | Average values of R_1, R_2, and hetNOE of S2–W1 region of FHD: apo, with target DNA, and with non-target DNA

DNA	R_1 [s^{-1}]	R_2 [s^{-1}]	hetNOE
No DNA	1.19 ± 0.02	12.47 ± 0.12	0.69 ± 0.01
Target DNA	0.63 ± 0.02	24.47 ± 1.10	0.81 ± 0.04
Non-target DNA	0.98 ± 0.01	13.87 ± 0.72	0.66 ± 0.04

While a previous study showed that loss of W2 (C-terminus) in FHD affects the target DNA binding[42], we found that deletion of the W2 region in FHD did not significantly change CSP profiles of FHD for target DNA interaction (Fig. 6). Instead, non-target DNA interactions were severely reduced by the W2 deletion. Based on these observations, it can be predicted that the interaction between the negatively charged phosphate of the DNA backbone and the positively charged residues in the FHD W2 region is important for non-target DNA binding. Consistent with expectations, our observation indicates that the W2 region plays a vital role in interacting with non-target DNA.

To further investigate the role of the W2 region and quantify binding characteristics, we analyzed K_d and exchange rates of FOXO4 FHD and the FHD_ΔW2 mutant with target and non-target DNA. We performed 2D lineshape analysis[53] on residues A107 and V167 (Supplementary Fig. 8),

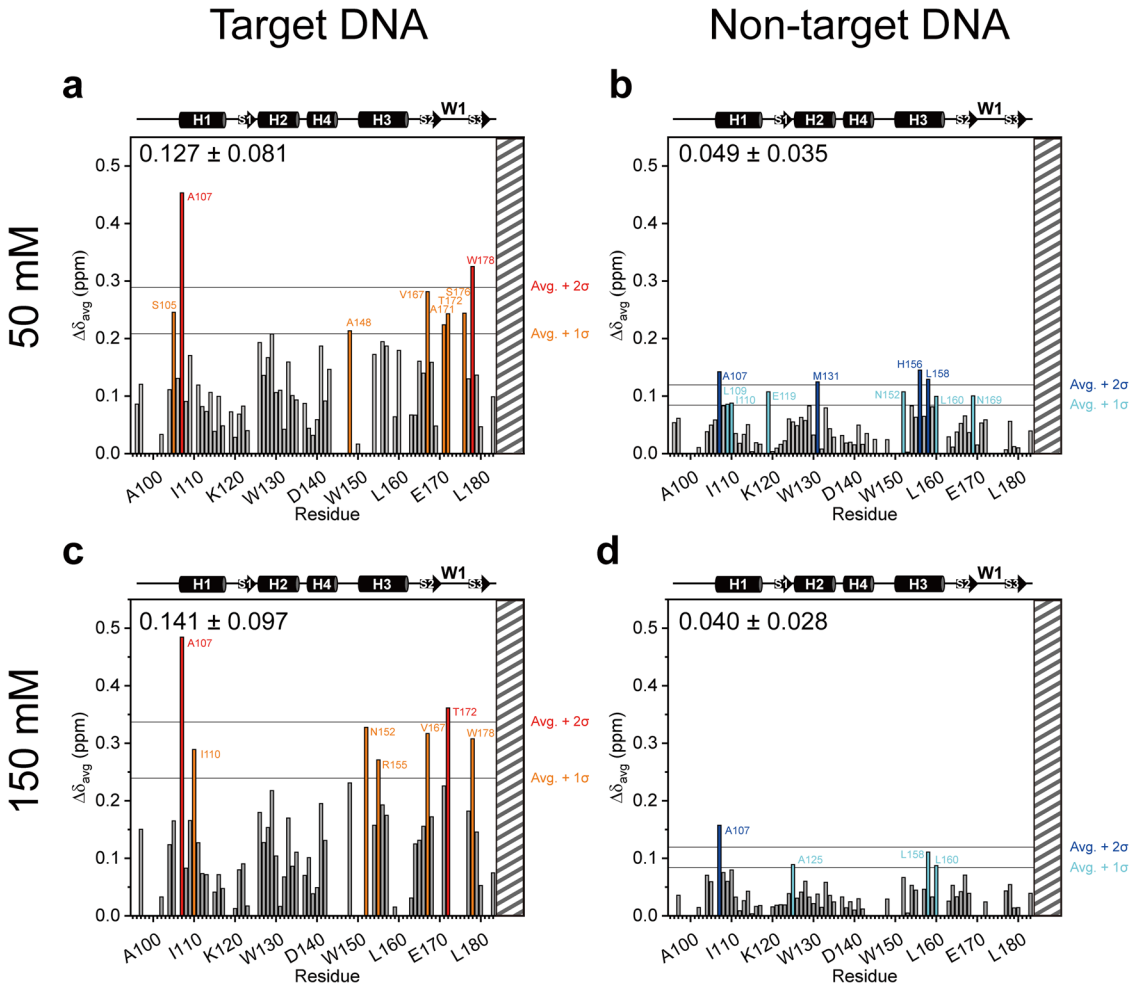

Fig. 6 | Average chemical shift perturbation ($\Delta\delta_{avg}$) of ^{15}N-labeled FOXO4 FHD_ΔW2. $\Delta\delta_{avg}$ of FOXO4 FHD_ΔW2 titrated at 50 mM NaCl (**a**, **b**) or 150 mM NaCl (**c**, **d**) with target (**a**, **c**) or non-target DNA (**b**, **d**). CSPs were calculated from the difference between FOXO4 FHD_ΔW2 and DNA ratios of 1:0 and 1:2. Residues with CSPs > 2 standard deviations larger than average are shown in red or blue, and residues > 1 standard deviation larger than average are shown in orange or cyan. Each average ± standard deviation is displayed in the upper left corner.

which exhibited distinct peak shifts across varying DNA concentrations, as shown in Fig. 4 and Supplementary Fig. 6. The disappearance of peaks under certain conditions led to uncertainty, particularly in K_d estimation (Supplementary Fig. 8). While the quantitative values should be interpreted cautiously due to these experimental limitations, our findings indicate that the target DNA–FHD system has a slower off-rate (k_{off}) than the non-target DNA–FHD system.

Under low salt conditions, both target and non-target DNA displayed comparable K_ds and k_{off}s for FHD WT. However, the target DNA–FHD system proved more resilient to high salt conditions and W2 deletion, while non-target DNA exhibited increased K_ds and k_{off} under these conditions. These findings corroborate that non-target DNA undergoes rapid exchange in response to high salt conditions and W2 deletion, while target DNA maintains slow exchange dynamics. Collectively, the 2D lineshape analysis supports the conclusion that non-target DNA binding to FHD is more dynamic and less stable than target DNA binding, with the W2 region playing a critical role in mediating non-target DNA interactions. These characteristics of different binding dynamics between target and non-target DNA suggest a mechanism that could facilitate efficient DNA scanning by FOXO4.

TFs scan DNA to reach target gene sequences. For this purpose, most TFs require a certain level of affinity with non-target DNA. According to the DNA loop formation theory[54], target DNA can be searched more quickly through the interaction between TFs and non-target DNA. The monkey-bar theory posits that TFs scan DNA preferentially through charge interactions between TFs and DNA, preventing it from straying too far from DNA, and making navigation efficient by using brachiation dynamics[52]. This aligns with the findings of this study, suggesting that the binding of non-target DNA and FHD occurs through electrostatic interactions, increases the flexibility of the FHD, and accelerates its exchange rate, further facilitating DNA scanning. This study provides detailed insight into the mechanism by which FOXO4 recognizes DNA and suggests a model of its role as a transcription initiator (Fig. 7).

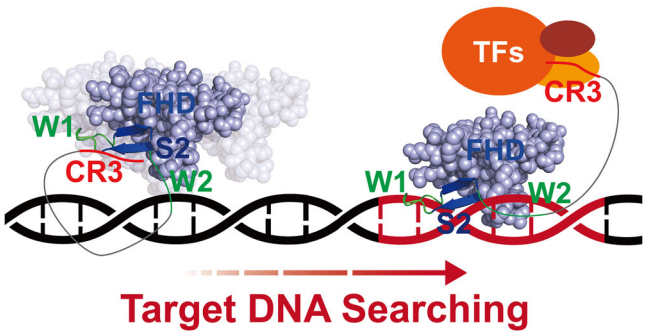

Fig. 7 | Role of FOXO4 as transcription initiator. FHD maintains non-target DNA contacts via electrostatic interactions through W2 region, while CR3 interacts with FHD. A more rigid FHD–DNA complex and released CR3 are observed at target DNA site.

Methods

Sample preparation

The full-length FOXO4 gene was obtained from Addgene (MA, USA). For the FHD (95–195 a.a.), it was inserted into the pET His6 tobacco etch virus (TEV) LIC cloning vector (2B–T) (a gift from Scott Gradia; Addgene plasmid #29666), and for the C-terminus conserved region 3 (469–505 a.a.; CR3), it was inserted into the pET His6 GST TEV LIC cloning vector (2G–T) (a gift from Scott Gradia, Addgene plasmid #29707). The FHD_ΔW2 (95–183 a.a.) was constructed by replacing residue 184 of the FHD vector with a terminal codon. These constructs were then introduced into *E. coli* BL21 (DE3) cells. All bacterial cultures were grown in Luria–Bertani (LB) medium at 37 °C until reaching an optical density of 0.6 at 600 nm. Induction was carried out by adding 0.5 mM IPTG, followed by a 20-h incubation at 18 °C. The proteins produced were purified using Ni-NTA column chromatography (GE Healthcare, IL, USA) and gel filtration chromatography using Hi-Load 16/600 Superdex 200 pg (GE Healthcare) on an AKTA pure system in a 20 mM HEPES, 50 mM NaCl, 1 mM dithiothreitol (DTT) buffer solution at pH 7.0 and 20 mM HEPES, 150 mM NaCl, 1 mM DTT buffer solution at pH 7.0. The GST tag was removed from the proteins using TEV protease. For ^{15}N-labeled samples used in ^{1}H–^{15}N HSQC experiments, cells were cultured in M9 minimal media with ^{15}N-labeled NH_4Cl. Similarly, ^{13}C/^{15}N double-labeled samples were created using ^{13}C-D-glucose and $^{15}NH_4Cl$. The protein expression and purification procedures were consistent with those used for LB-cultured proteins. All DNA molecules were purchased from Integrated DNA Technologies. The target DNA (5′-GCGTAAACAACGC-3′) and non-target DNA (5′-GTCTGTCAGTCTG-3′) were mixed with their complementary strands. The mixed DNAs were denatured at 95 °C for 10 min and then annealed for 1 h at 25 °C.

Nuclear magnetic resonance experiments

NMR experiments were conducted using 800, 900, and 1200 MHz Bruker (MA, USA) NMR spectrometers with cryogenic probes located in KBSI Ochang, as well as a Bruker 600 MHz NMR spectrometer with a prodigy probe in GIST Gwangju. Experiments, except for physiological salt conditions (150 mM NaCl), were carried out in a buffer solution containing 20 mM HEPES at pH 7.0, 50 mM NaCl, and 1 mM DTT at 25 °C. The data obtained from NMR experiments were processed using the Topspin software from Bruker and analyzed using POKY software[55]. The amide nitrogens and protons of FHD have been assigned previously[56]. For the ^{1}H–^{15}N HSQC titration experiments, samples without labels were mixed with labeled samples at progressively increasing concentrations. In competition experiments, the concentration of DNA was increased while maintaining the same ratio of FHD and CR3. $\Delta\delta_{avg}s$ were calculated using the provided equation:

$$\Delta\delta\mathrm{avg} = \sqrt{(\Delta\delta\mathrm{H})^2 + (\Delta\delta\mathrm{N}/5.88)^2}$$

where $\Delta\delta_H$ and $\Delta\delta_N$ represent the chemical shift changes of the amide proton and the nitrogen, respectively.

For PRE experiments, CR3 was labeled with MTSL[57]. The experiment was conducted with NMR buffer (except the DTT) under conditions where the ratio of ^{15}N-labeled FHD to MTSL-labeled CR3 was 1:1, and the DNA ratio was 2:1. To obtain the spectrum of the diamagnetic state, a solution containing 0.5 mM of ascorbic acid from a 250 mM stock was introduced into the sample. This mixture was then incubated for 3 h at 25 °C before conducting NMR measurements. To perform PRE measurements, two sets of ^{1}H-^{15}N HSQC spectra were obtained from the identical sample, one before and one after reducing the spin-label. The intensities of peaks were quantified and presented as the ratio of intensities between the oxidized ($I_{paramagnetic}$) and reduced states ($I_{diamagnetic}$). For PRE $^{1}H_N$–Γ_2 measurements, samples comprising the FOXO4 FHD–DNA complex and MTSL-labeled CR3 were analyzed using two-dimensional ^{1}H–^{15}N correlation spectra with a 1.2 GHz NMR instrument (KBSI, Ochang). The pulse sequence was provided by Prof. Iwahara, University of Texas Medical Branch[58]. Two-time points with a difference of 10 ms were used. The $^{1}H_N$–Γ_2 values were then calculated according to the established method[58].

^{15}N relaxation measurements

The ^{15}N relaxation measurements were conducted at a temperature of 25 °C using a Bruker 900 MHz NMR spectrometer with a cryogenic probe (KBSI, Ochang). The sampling of R_1 involved employing inversion recovery delays of 30, 60, 100, 200, 400, 600, 800, 1000, 1200, and 1500 ms. The sampling of R_2 involved employing CPMG delays of 16.96, 33.92, 50.88, 67.84, 101.76, 135.68, 169.6, 203.2, 254.4, and 339.2 ms. In the hetNOE experiment, the saturation period for the proton (^{1}H) was set at 5 s. The acquisition of All two-dimensional spectra was performed sequentially in matrices of 2048 (^{1}H) × 256 (^{15}N) complex points, with an inter-scan delay of 5 s. Relaxation rate constants were determined using POKY by fitting the decay of peak height to a single exponential function as a function of the relaxation delay[55]. The hetNOE values were determined by calculating peak height ratios between pairs of spectra using a POKY script. The τ_c was calculated by this equation[59,60]:

$$\tau_c = \left(\frac{1}{4\pi\nu_N}\right)\sqrt{\left(6\frac{R_1}{R_2} - 7\right)}$$

where ν_N is the resonance frequency of ^{15}N in Hz. We calculated the $\tau_c s$ by considering the commonly available residues (34 residues) in all states and then averaging the τ_c for each residue.

Isothermal titration calorimetry (ITC)

ITC experiments were performed in 20 mM HEPES, 50 mM NaCl, and 1 mM DTT buffer solution at pH 7.0 using a Nano-ITC SV instrument (TA Instruments, DE, USA). Twenty-four aliquots of 10 μL of 200 μM FHD were titrated from the syringe into 10 μM target or non-target DNA in the cell at 25 °C. The stirring speed was maintained at 300 rpm, with a 300 s interval between titrations. Data were analyzed using NanoAnalyze software (TA Instruments), and the K_d and stoichiometry (N) were determined by fitting the data to an independent binding model.

2D lineshape analysis of two-state binding

^{1}H–^{15}N HSQC titration spectra were analyzed using TITAN v1.6[53]. For our analysis, a two-state binding model was employed to describe the interaction between the free FOXO4 FHD protein (P) and a DNA ligand (L), representing either target or non-target DNA, to form the bound state PL:

$$\mathrm{P} + \mathrm{L} \rightleftharpoons \mathrm{PL}$$

TITAN software was used to fit the titration spectra globally, allowing extraction of key model parameters, including K_d and k_{off}, for both target and non-target DNA. Four to seven spectra were collected at varying DNA concentrations. Residues A107 and V167 were selected for analysis based on their significant chemical shift changes observed during titration.

Data availability

All data that support the findings of this study are available in the article and Supplementary information. The protein structure from accession codes 3L2C (FOXO4 FHD–DNA complex) was obtained from the PDB at https://www.rcsb.org/. The assignment is found in Biological Magnetic Resonance Data Bank (http://www.bmrb.wisc.edu/) with the BMRB accession code 52558. All other data are available from the corresponding author upon reasonable request.

Received: 11 April 2024; Accepted: 24 October 2024;
Published online: 01 November 2024

References

1. Schmidt, H. G., Sewitz, S., Andrews, S. S. & Lipkow, K. An integrated model of transcription factor diffusion shows the importance of intersegmental transfer and quaternary protein structure for target site finding. *PLoS ONE* **9**, e108575 (2014).
2. Lambert, S. A. et al. The human transcription factors. *Cell* **172**, 650–665 (2018).
3. Weigel, D. & Jäckle, H. The fork head domain: a novel DNA binding motif of eukaryotic transcription factors? *Cell* **63**, 455–456 (1990).
4. Kaufmann, W. K. & Paules, R. S. DNA damage and cell cycle checkpoints. *FASEB J.* **10**, 238–247 (1996).
5. Marsden, I., Jin, C. & Liao, X. Structural changes in the region directly adjacent to the DNA-binding helix highlight a possible mechanism to explain the observed changes in the sequence-specific binding of winged helix proteins. *J. Mol. Biol.* **278**, 293–299 (1998).
6. Nagaich, A. K. et al. p53-induced DNA bending and twisting: p53 tetramer binds on the outer side of a DNA loop and increases DNA twisting. *Proc. Natl Acad. Sci. USA* **96**, 1875–1880 (1999).
7. Brownawell, A. M., Kops, G. J., Macara, I. G. & Burgering, B. M. Inhibition of nuclear import by protein kinase B (Akt) regulates the subcellular distribution and activity of the forkhead transcription factor AFX. *Mol. Cell. Biol.* **21**, 3534–3546 (2001).
8. Birkenkamp, K. U. & Coffer, P. J. Regulation of cell survival and proliferation by the FOXO (forkhead box, class O) subfamily of Forkhead transcription factors. *Biochem. Soc. Trans.* **31**, 292–297 (2003).
9. Accili, D. & Arden, K. C. FoxOs at the crossroads of cellular metabolism, differentiation, and transformation. *Cell* **117**, 421–426 (2004).
10. Essers, M. A. G. et al. FOXO transcription factor activation by oxidative stress mediated by the small GTPase Ral and JNK. *EMBO J.* **23**, 4802–4812 (2004).
11. Barthel, A., Schmoll, D. & Unterman, T. G. FoxO proteins in insulin action and metabolism. *Trends Endocrinol. Metab.* **16**, 183–189 (2005).
12. de Keizer, P. L. J. et al. Activation of forkhead box O transcription factors by oncogenic BRAF promotes p21Cip1-dependent senescence. *Cancer Res.* **70**, 8526–8536 (2010).
13. van den Berg, M. C. W. et al. The small GTPase RALA controls c-Jun N-terminal kinase-mediated FOXO activation by regulation of a JIP1 scaffold complex. *J. Biol. Chem.* **288**, 21729–21741 (2013).
14. Wang, Y., Zhou, Y. & Graves, D. T. FOXO transcription factors: their clinical significance and regulation. *BioMed. Res. Int.* **2014**, 925350 (2014).
15. Baar, M. P. et al. Targeted apoptosis of senescent cells restores tissue homeostasis in response to chemotoxicity and aging. *Cell* **169**, 132–147.e16 (2017).
16. Carter, M. E. & Brunet, A. FOXO transcription factors. *Curr. Biol.* **17**, R113–R114 (2007).
17. Myatt, S. S. & Lam, E. W. F. The emerging roles of forkhead box (Fox) proteins in cancer. *Nat. Rev. Cancer* **7**, 847–859 (2007).
18. van der Vos, K. E. & Coffer, P. J. The extending network of FOXO transcriptional target genes. *Antioxid. Redox Signal.* **14**, 579–592 (2011).
19. Matsuzaki, H. et al. Acetylation of FOXO1 alters its DNA-binding ability and sensitivity to phosphorylation. *Proc. Natl Acad. Sci. USA* **102**, 11278–11283 (2005).
20. Brenkman, A. B., de Keizer, P. L. J., van den Broek, N. J. F., Jochemsen, A. G. & Burgering, B. M. T. Mdm2 induces mono-ubiquitination of FOXO4. *PLoS ONE* **3**, e2819 (2008).
21. Bartholome, A., Kampkötter, A., Tanner, S., Sies, H. & Klotz, L. O. Epigallocatechin gallate-induced modulation of FoxO signaling in mammalian cells and *C. elegans*: FoxO stimulation is masked via PI3K/Akt activation by hydrogen peroxide formed in cell culture. *Arch. Biochem. Biophys.* **501**, 58–64 (2010).
22. Wang, F. et al. Structures of KIX domain of CBP in complex with two FOXO3a transactivation domains reveal promiscuity and plasticity in coactivator recruitment. *Proc. Natl Acad. Sci. USA* **109**, 6078–6083 (2012).
23. Daitoku, H., Sakamaki, J. I. & Fukamizu, A. Regulation of FoxO transcription factors by acetylation and protein-protein interactions. *Biochim. Biophys. Acta* **1813**, 1954–1960 (2011).
24. Biggs, W. H. 3rd, Cavenee, W. K. & Arden, K. C. Identification and characterization of members of the FKHR (FOX O) subclass of winged-helix transcription factors in the mouse. *Mamm. Genome* **12**, 416–425 (2001).
25. Furuyama, T., Nakazawa, T., Nakano, I. & Mori, N. Identification of the differential distribution patterns of mRNAs and consensus binding sequences for mouse DAF-16 homologues. *Biochem. J.* **349**, 629–634 (2000).
26. Brent, M. M., Anand, R. & Marmorstein, R. Structural basis for DNA recognition by FoxO1 and its regulation by posttranslational modification. *Structure* **16**, 1407–1416 (2008).
27. Boura, E., Rezabkova, L., Brynda, J., Obsilova, V. & Obsil, T. Structure of the human FOXO4-DBD-DNA complex at 1.9 Å resolution reveals new details of FOXO binding to the DNA. *Acta Crystallogr. D* **66**, 1351–1357 (2010).
28. Kim, J., Ahn, D. & Park, C.-J. FOXO4 transactivation domain interaction with forkhead DNA binding domain and effect on selective DNA recognition for transcription initiation. *J. Mol. Biol.* **433**, 166808 (2021).
29. Mathiasen, L. et al. The flexibility of a homeodomain transcription factor heterodimer and its allosteric regulation by DNA binding. *FEBS J.* **283**, 3134–3154 (2016).
30. Zhang, Y., Larsen, C. A., Stadler, H. S. & Ames, J. B. Structural basis for sequence specific DNA binding and protein dimerization of HOXA13. *PLoS ONE* **6**, e23069 (2011).
31. Krois, A. S., Dyson, H. J. & Wright, P. E. Long-range regulation of p53 DNA binding by its intrinsically disordered N-terminal transactivation domain. *Proc. Natl Acad. Sci. USA* **115**, E11302–E11310 (2018).
32. Bragdon, M. D. J. et al. Cooperative assembly confers regulatory specificity and long-term genetic circuit stability. *Cell* **186**, 3810–3825.e18 (2023).
33. Datta, R. R. & Rister, J. The power of the (imperfect) palindrome: sequence-specific roles of palindromic motifs in gene regulation. *BioEssays* **44**, e2100191 (2022).
34. Li, J. et al. Mechanism of forkhead transcription factors binding to a novel palindromic DNA site. *Nucleic Acids Res.* **49**, 3573–3583 (2021).
35. Wang, B., Lin, D., Li, C. & Tucker, P. Multiple domains define the expression and regulatory properties of Foxp1 forkhead transcriptional repressors. *J. Biol. Chem.* **278**, 24259–24268 (2003).
36. Li, S., Weidenfeld, J. & Morrisey, E. E. Transcriptional and DNA binding activity of the Foxp1/2/4 family is modulated by heterotypic and homotypic protein interactions. *Mol. Cell. Biol.* **24**, 809–822 (2004).
37. Stroud, J. C. et al. Structure of the forkhead domain of FOXP2 bound to DNA. *Structure* **14**, 159–166 (2006).
38. Wu, Y. et al. FOXP3 controls regulatory T cell function through cooperation with NFAT. *Cell* **126**, 375–387 (2006).
39. Bourgeois, B. et al. Multiple regulatory intrinsically disordered motifs control FOXO4 transcription factor binding and function. *Cell Rep.* **36**, 109446 (2021).
40. Softley, C. A., Bostock, M. J., Popowicz, G. M. & Sattler, M. Paramagnetic NMR in drug discovery. *J. Biomol. NMR* **74**, 287–309 (2020).
41. Iwahara, J. & Clore, G. M. Detecting transient intermediates in macromolecular binding by paramagnetic NMR. *Nature* **440**, 1227–1230 (2006).
42. Obsil, T. & Obsilova, V. Structural basis for DNA recognition by FOXO proteins. *Biochim. Biophys. Acta* **1813**, 1946–1953 (2011).
43. Qureshi, N. S. et al. NMR structure of the *Vibrio vulnificus* ribosomal protein S1 domains D3 and D4 provides insights into molecular

recognition of single-stranded RNAs. *Nucleic Acids Res.* **49**, 7753–7764 (2021).
44. Li, Q., Ng, H. Q. & Kang, C. Secondary structure and topology of the transmembrane domain of Syndecan-2 in detergent micelles. *FEBS Lett.* **593**, 554–561 (2019).
45. Bourgeois, B. & Madl, T. Regulation of cellular senescence via the FOXO4-p53 axis. *FEBS Lett.* **592**, 2083–2097 (2018).
46. Wang, X. et al. Negatively charged, intrinsically disordered regions can accelerate target search by DNA-binding proteins. *Nucleic Acids Res.* **51**, 4701–4712 (2023).
47. Regan, M. C. et al. Structural and dynamic studies of the transcription factor ERG reveal DNA binding is allosterically autoinhibited. *Proc. Natl Acad. Sci. USA* **110**, 13374–13379 (2013).
48. Currie, S. L. et al. Structured and disordered regions cooperatively mediate DNA-binding autoinhibition of ETS factors ETV1, ETV4 and ETV5. *Nucleic Acids Res.* **45**, 2223–2241 (2017).
49. Luscombe, N. M., Laskowski, R. A. & Thornton, J. M. Amino acid-base interactions: a three-dimensional analysis of protein-DNA interactions at an atomic level. *Nucleic Acids Res.* **29**, 2860–2874 (2001).
50. Kalodimos, C. G. et al. Structure and flexibility adaptation in nonspecific and specific protein-DNA complexes. *Science* **305**, 386–389 (2004).
51. Boura, E. et al. Both the N-terminal loop and wing W2 of the forkhead domain of transcription factor Foxo4 are important for DNA binding. *J. Biol. Chem.* **282**, 8265–8275 (2007).
52. Vuzman, D. & Levy, Y. DNA search efficiency is modulated by charge composition and distribution in the intrinsically disordered tail. *Proc. Natl Acad. Sci. USA* **107**, 21004–21009 (2010).
53. Waudby, C., Ramos, A., Cabrita, L. D. & Christodoulou, J. Two-dimensional NMR lineshape analysis. *Sci. Rep.* **6**, 24826 (2016).
54. Shin, J. & Kolomeisky, A. B. Facilitation of DNA loop formation by protein-DNA non-specific interactions. *Soft Matter* **15**, 5255–5263 (2019).
55. Lee, W., Rahimi, M., Lee, Y. & Chiu, A. POKY: a software suite for multidimensional NMR and 3D structure calculation of biomolecules. *Bioinformatics* **37**, 3041–3042 (2021).
56. Weigelt, J., Climent, I., Dahlman-Wright, K. & Wikström, M. 1H, 13C and 15N resonance assignments of the DNA binding domain of the human forkhead transcription factor AFX. *J. Biomol. NMR* **17**, 181–182 (2000).
57. Sjodt, M. & Clubb, R. T. Nitroxide labeling of proteins and the determination of paramagnetic relaxation derived distance restraints for NMR studies. *Bio Protoc.* **7**, e2207 (2017).
58. Iwahara, J., Tang, C. & Marius Clore, G. Practical aspects of (1)H transverse paramagnetic relaxation enhancement measurements on macromolecules. *J. Magn. Reson.* **184**, 185–195 (2007).
59. Kay, L. E., Torchia, D. A. & Bax, A. Backbone dynamics of proteins as studied by 15N inverse detected heteronuclear NMR spectroscopy: application to staphylococcal nuclease. *Biochemistry* **28**, 8972–8979 (1989).
60. de Medeiros, L. N. et al. Backbone dynamics of the antifungal Psd1 pea defensin and its correlation with membrane interaction by NMR spectroscopy. *Biochim. Biophys. Acta* **1798**, 105–113 (2010).

Acknowledgements

We thank the high-field NMR facility at the Korea Basic Science Institute (KBSI, Ochang) and GIST Advanced Institute of Instrumental Analysis (GAIA, Gwangju) for allowing us to use their NMR spectrometers. We thank Dr. Melissa Stauffer of Scientific Editing Solutions for editing the manuscript. This work was supported by the National Research Foundation of Korea [grant numbers 2021R1A2C1004669 and RS-2024-00411137], which was funded by the Korean government (MSIT) and the KBSI under the R&D program [project number A412550] and supervised by the Ministry of Science and ICT, Korea. This work is dedicated to the late Prof. Joon-Hwa Lee of Gyeongsang National University.

Author contributions

D.K.: Conceptualization, formal analysis, investigation, visualization, writing-original draft, writing-review & editing. M.J.Y.: Formal analysis, investigation, validation, writing-original draft, writing-review & editing. H.-K.C.: Analysis, writing-review & editing. C.-J.P.: Conceptualization, funding acquisition, supervision, writing-review & editing.

Competing interests

The authors declare no competing interests.

Additional information

Supplementary information The online version contains supplementary material available at https://doi.org/10.1038/s42003-024-07133-1.

Correspondence and requests for materials should be addressed to Chin-Ju Park.

Peer review information *Communications Biology* thanks Mahavir Singh, Yoshifumi Nishimura, and the other, anonymous, reviewer for their contribution to the peer review of this work. Primary Handling Editors: Luciano Abriata and Mengtan Xing.